Local conductance spectra of itinerant ferromagnetic SrRuO$_3$ through break junction

Hiroshi Kambara[1]*, Yūki Obinata[1], Kenichi Tenya[1], and Hiroyuki Tsujii[2]

[1] Department of Physics, Faculty of Education, Shinshu University, Nagano 380-8544, Japan

[2] Department of Physics, Faculty of Education, Kanazawa University, Kanazawa 920-1192, Japan

We have measured the local differential conductance spectra (dI/dV - V) of an itinerant ferromagnet composed of polycrystalline SrRuO$_3$ using the mechanically controllable break junction technique. Below the material's Curie temperature (T_C = 160 K), characteristic peak or dip conductance spectra are observed. The characteristic energy scale is comparable to the exchange spin splitting energy that is based on ferromagnetic band calculations. Both the peak and dip spectral shapes are explained based on the itinerant ferromagnetic characteristics of SrRuO$_3$ in terms of spin-dependent transmission, which is similar to the giant magnetoresistance mechanism.

1. Introduction

Electronic transport characteristics in bulk systems usually reflect the average electronic properties of condensed matter. Recently, Ienaga *et al.*[1] observed zero-bias asymmetric anomalies in the differential conductance in ferromagnetic Ni nanoconstrictions produced by the mechanically controllable break junction (MCBJ) technique.[2] These anomalies were explained in terms of the Fano effect, which originates from the Kondo effect. The Kondo effect is known to be observed in dilute magnetic alloys (e.g., AuFe), in which a small number of magnetic atoms (iron) exist as impurities in a pure metal (gold) and antiferromagnetic *s* - *d* interactions between the localized spins and conduction electrons play an important role.[3] It is therefore remarkable that the Kondo effect has been revealed in a ferromagnetic Ni wire. One important aspect of this MCBJ experiment[1] was the measurement of the local transport characteristics of the nanoconstrictions of the Ni wire rather than that of the bulk characteristics. This showed that by applying a bias voltage with focus on a nanoscale region, it is possible to discover new transport phenomena hidden in a bulk material.

Strontium ruthenate compounds of the Ruddlesden-Popper series, such as Sr$_{n+1}$Ru$_n$O$_{3n+1}$, show many attractive properties. For example, Sr$_2$RuO$_4$ (n = 1) is now widely believed to

*E-mail:kambara@shinshu-u.ac.jp

be a chiral p-wave spin-triplet superconductor with time-reversal symmetry-breaking properties,[4,5] and $Sr_3Ru_2O_7$ ($n = 2$) shows metamagnetism with a quantum critical point.[6,7] For $n = \infty$, $SrRuO_3$ is an itinerant ferromagnetic metal with a Curie temperature (T_C) of 160 K.[8,9] The bulk perovskite $SrRuO_3$ structure is orthorhombic at temperatures below 550 °C.[10] Because of the material's good lattice matching properties, thin films of $SrRuO_3$ are often used as electrodes in heteroepitaxial devices; moreover, $SrRuO_3$ is one of only a few oxides that show metallic conductivity without doping. Many experimental and theoretical studies of $SrRuO_3$ have been carried out to date, but MCBJ experiments on $SrRuO_3$ junctions have not yet been reported. Using the MCBJ technique, it is possible to apply a wide range of bias voltages to a $SrRuO_3$ junction to investigate the local electronic states of $SrRuO_3$. It is also possible to measure the local electronic states of the material, both below T_C and above T_C, because of its moderate T_C value.

In this paper, we present results of local differential conductance spectra (dI/dV - V) measurements of an itinerant ferromagnetic oxide, $SrRuO_3$ ($T_C = 160$ K), using the MCBJ technique at temperatures above and below the material T_C. The differential conductance spectra measured in the ferromagnetic and paramagnetic states over a wide junction conductance range enables us to extract the electronic states of ferromagnetically ordered states.

2. Experimental methods

Polycrystalline $SrRuO_3$ samples were prepared by a conventional solid-state reaction method using $SrCO_3$ and RuO_2 as starting materials. After careful mixing, the materials were shaped into pellets and sintered at 1100 °C in air. After subsequent crushing of the pellets, the above process was then repeated. Scanning electron microscopy (SEM) images of the sample surface show numerous sintered grains with sizes of approximately 0.1–1 μm [Fig. 1(c)]. The quality of the test samples was checked using bulk resistivity - temperature (ρ - T) measurements [Fig. 1(d)], which show a clear kink at 163 K that reflects the ferromagnetic transition observed in previous reports.[8,11] The ρ - T measurements are described in more detail later. The MCBJ experiments were then performed using five pieces of $SrRuO_3$. Each piece for the MCBJ experiments was cut to a size of $\sim 3 \times 1 \times 0.5$ mm^3, with a notch located at the center of the piece for the breakage, as shown in Fig. 1(a). The piece was electrically isolated from a phosphor bronze bending beam (0.3 mm thick) using a sheet of cigarette paper and was then glued to the beam using Stycast 2850FT epoxy. The differential conductance (dI/dV - V) was measured using a quasi-four-probe lock-in technique at an ac modulation frequency of 89.3 Hz and amplitudes of $\sim$ 0.3–3 mV. In this case, "quasi-" means that the current and voltage

lines were glued together on the sample surface using the same droplet of silver epoxy [Fig. 1(a)]. Because the break junction resistance ($\sim 10^2$–10^4 Ω) is much higher than the contact resistance between the silver epoxy and the sample, this method is regarded as the standard method. The measurements were carried out at less than 1×10^{-3} Pa at temperatures ranging from 77 to 200 K using liquid nitrogen and dry ice. In this paper, we report the data from three of the samples of SrRuO$_3$ (samples S1, S2, and S3) because the other samples also showed similar results to S1-S3.

3.   Results

The bulk ρ - T curve of SrRuO$_3$ shows a clear ferromagnetic transition kink at 163 K (T_C), as shown in Fig. 1(d). The reduction in resistivity below T_C is regarded as the suppression of electron scattering caused by spin fluctuations.[12] The magnitude of ρ of the polycrystalline sample, however, is approximately seven times larger than that of a single-crystal material.[8] Therefore, the mean free path of this sample is estimated to be much shorter than that of the single crystal. In this case, the values of the mean free path l of the sample are estimated to be $l(77$ K$) \simeq 0.3$ nm and $l(200$ K$) \simeq 0.2$ nm by applying the Drude formula for the measured bulk resistivity with reference to the estimation of Allen *et al.*[8] These estimates of l are reasonable because the room-temperature mean free path for a mixed single crystal of Sr$_{0.47}$Ca$_{0.53}$RuO$_3$, which shows a similar resistivity to the present sample, was also estimated to be in the range of only 0.2–0.3 nm.[13]

Figures 2(a) and 2(b) show a wide range of differential conductance spectra (dI/dV - V) from the SrRuO$_3$ sample S1 at temperatures of 77 K ($T < T_C$) and 200 K ($T > T_C$), respectively. The spectra show peak or dip structures at approximately zero bias voltage at 77 K ($T < T_C$), while they are almost constant at 200 K ($T > T_C$). Therefore, the differences between the spectra with respect to temperature suggest that ferromagnetism plays an important role in the conductance spectra. Here, we note that a conductance of 1×10^{-4} S corresponds to $\sim 1G_0$; the quantum conductance $G_0 = 2e^2/h$ ($1/G_0 \approx 12.9$ kΩ), where e is the electronic charge and h is Planck's constant. Therefore, the conductance spectra shown here were obtained in the contact region, although $1G_0$ for SrRuO$_3$ does not necessarily indicate a specific conductance observed in, for example, a gold atomic chain.[14, 15]

Figures 3(a)-3(f) show the normalized dI/dV characteristics of the SrRuO$_3$ samples S1, S2, and S3, and the data of nonmagnetic copper for comparison [Figs. 3(m) and 3(n)]. The peak and dip structures of dI/dV - V in the ferromagnetic states are clear. To show the kink structures of dI/dV - V more clearly, we show d^2I/dV^2 - V spectra, which are the numerical

derivatives of raw dI/dV data with respect to V. The d^2I/dV^2 - V spectra show a clear deviation at approximately ±0.2 V in Figs. 3(g)-3(i) at 77 K ($< T_C$). In contrast, no anomalous features are observed in Figs. 3(j)-3(l) at 200 K ($> T_C$). Thus, the characteristic energy scales of the peaks or dips ($E_{p,d}$) are considered to be approximately 0.2 eV. We cannot immediately evaluate $E_{p,d}$ from theoretical band calculations.[16–19] Note, however, that $E_{p,d}$ is of the same order as the calculated exchange spin splitting energy of $\Delta_{ex} \simeq 0.65$ eV.[16] Broadly speaking, Δ_{ex} is the splitting energy that occurs between the majority and minority band peaks across the Fermi energy E_F of this compound. Therefore, the conductance is variable and may increase or decrease when we increase the bias voltage from zero up to $\approx \Delta_{ex}/e$ in the ferromagnetic state. The origins of these two kinds of spectral shapes are discussed later.

To see the temperature variation of dI/dV - V, we study the data of sample S1 shown in Fig. 4. As the temperature increases, the conductance also increases because of the difference in the thermal expansion coefficient between the sample ($SrRuO_3$) and the bending beam (phosphor bronze) shown in Fig. 1(a). However, we can see clear spectral variations in the normalized dI/dV - V data. Figure 4(b) shows clear changes in the shape of spectra from a dip (low dI/dV at $T < T_C$) to a peak (high dI/dV at $T < T_C$) and finally to a flat shape ($T > T_C$). This result supports the idea that the peak or dip structures originate from ferromagnetism.

4. Discussion

The experimental results are summarized as follows. At temperatures below T_C, the dI/dV - V spectra show peak or dip structures around zero bias voltage up to energy scales of $E_{p,d} \simeq 0.2$ eV. In contrast, these peak or dip structures disappear at temperatures above T_C.

We consider the origins of the peak and dip structures in the ferromagnetic states. In this experimental case, the mean free path l is estimated to be too small and comparable to the lattice constant of this compound.[10] Therefore, electron transport is not ballistic but diffusive. Furthermore, junctions are not ideal point contacts but are several conduction paths with several grains because of the polycrystalline nature of the sample, as shown in Fig. 1(c). We roughly estimate, however, the effective junction size on the basis of a point contact model connected through a circular orifice of diameter d. In a diffusive regime where $l \ll d$, contact resistance is expressed as the Maxwell resistance $R_M = \frac{\rho}{d}$.[20,21] Thus, the effective junction sizes in the conductance range of $\sim 5 \times 10^{-4}$–1×10^{-2} S are estimated to be ~ 3–55 nm at 77 K, and ~ 4.5–90 nm at 200 K. Taking the Ru-Ru distance of 0.39 nm[10] into account, junctions contain ~ 50–1.6×10^4, and ~ 100–4.2×10^4 RuO_6 octahedra units at 77 and 200 K, respectively. Here we note that a magnetic domain size of ~ 200 nm[22] is on the same

order as grain size. Therefore, the junction sizes are smaller than the domain size. We also note that the magnetic domain wall size is relatively small (approximately 3 nm[22] or smaller than 10 nm[23]), as determined by thin-film experiments, reflecting a highly cohesive field of $SrRuO_3$.[24]

Here, we regard the junction as a type of giant magnetoresistance (GMR) device.[25–27] GMR is ascribed to spin-dependent electrical transport phenomena that show low (high) resistance between the parallel (antiparallel) spin configurations of ferromagnetic devices. The mechanism is explained based on spin-dependent transmission and the density of states (DOS) by assuming elastic scattering, from which the spin-flop scattering is absent. Figures 5(c)-5(f) show schematic diagrams of the DOS [$D(E)$] of the parallel and antiparallel spin configurations of $SrRuO_3$ under zero and finite bias voltage conditions ($V \sim \Delta_{ex}/e$). The tendency of the differential conductance dI/dV to increase or decrease is roughly estimated using an integral ($I = \int \frac{dI}{dV} dV$) because I is proportional to an overlapping area of $D(E)_1$ and $D(E)_2$ (1, 2: electrode index). If the overlapping area increases at a specific rate [$\propto D(E_F)$] with increasing bias voltage, then dI/dV = constant, which thus obeys Ohm's law. However, if the overlapping area increases at a rate that is higher than the specified rate [$\propto D(E_F)$], then dI/dV also increases, and vice versa. Here, we suppose that we increase the bias voltage from zero to $\sim \Delta_{ex}/e$ in the parallel spin configuration [Figs. 5(c) and 5(d)]. Then, the overlapping area of the up-spin part hardly increases because there are hardly any empty states left above E_F to which the high-energy electrons can be transferred. In addition, the overlapping area of the down-spin part does not increase either when compared with the value of $\sim D(E_F) \cdot (eV)$ [see the overlapping area indicated by hatching in Fig. 5(d)]; therefore, dI/dV decreases. In the antiparallel configuration [Figs. 5(e) and 5(f)], the overlapping area of the up-spin part hardly increases similarly to that in the parallel configuration; however, the overlapping area of the down-spin part increases at a rate higher than the specified rate [$\propto D(E_F)$] in this case [see the overlapping area indicated by hatching in Fig. 5(f)]. We note here that the contribution of the up-spin part is basically small in this model; thus, the contribution of the down-spin part is dominant for the total dI/dV. Therefore, the total dI/dV increases from zero to $\sim \Delta_{ex}/e$ in the antiparallel configuration. The peak (dip) structure of dI/dV can therefore be qualitatively explained using the GMR model. It suggests that the ferromagnetic grain-grain MCBJ contacts behave as a spin-dependent transmission device, although the transport phenomena are not real tunneling phenomena. These results are also in good agreement with the results of the *ab initio* calculations of the Ni magnetic point contact, in which dI/dV - V shows a peak in the parallel spin configuration and a dip in the antiparallel spin configuration.[28]

5. Conclusions

We have measured the local differential conductance spectra (dI/dV - V) of polycrystalline SrRuO$_3$ samples in wide bias voltage ranges using the MCBJ technique. Below the Curie temperature T_C, characteristic peak or dip structures were observed in the dI/dV - V spectra, reflecting the material's ferromagnetism. No characteristic spectra were observed above T_C. We assume that the junctions are formed with several SrRuO$_3$ grain contacts. Using the analogy of the GMR mechanism, the peak (dip) structures of the dI/dV spectra can be qualitatively explained. By taking into account the spin-dependent DOS for transmission without spin-flop, the peak (dip) structures are expected to occur between parallel (antiparallel) domains. The characteristic energy scales of the dI/dV - V spectra for both the peak and dip structures are $E_{p,d} \simeq 0.2$ eV, which is comparable to the exchange splitting energy from the ferromagnetic band calculation ($\Delta_{ex} \simeq 0.65$ eV). These results suggest that the observed transport phenomena can be attributed to the itinerant ferromagnetic characteristics of SrRuO$_3$.

Acknowledgments

References

1) K. Ienaga, N. Nakashima, Y. Inagaki, H. Tsujii, S. Honda, T. Kimura, and T. Kawae, Phys. Rev. B **86**, 064404 (2012).

2) N. Agraït, A. L. Yeyati, and J. M. van Ruitenbeek, Phys. Rep. **377**, 81 (2003).

3) J. Kondo, Prog. Theor. Phys. **32**, 37 (1964).

4) A. P. Mackenzie and Y. Maeno, Rev. Mod. Phys. **75**, 657 (2003).

5) Y. Maeno, S. Kittaka, T. Nomura, S. Yonezawa, and K. Ishida, J. Phys. Soc. Jpn. **81**, 011009 (2012).

6) S. A. Grigera, P. Gegenwart, R. A. Borzi, F. Weickert, A. J. Schofield, R. S. Perry, T. Tayama, T. Sakakibara, Y. Maeno, A. G. Green, and A. P. Mackenzie, Science **306**, 1154 (2004).

7) R. A. Borzi, S. A. Grigera, J. Farrell, R. S. Perry, S. J. S. Lister, S. L. Lee, D. A. Tennant, Y. Maeno, and A. P. Mackenzie, Science **315**, 214 (2007).

8) P. B. Allen, H. Berger, O. Chauvet, L. Forro, T. Jarlborg, A. Junod, B. Revaz, and G. Santi, Phys. Rev. B **53**, 4393 (1996).

9) G. Koster, L. Klein, W. Siemons, G. Rijnders, J. S. Dodge, C.-B. Eom, D. H. A. Blank, and M. R. Beasley, Rev. Mod. Phys. **84**, 253 (2012).

10) K. J. Choi, S. H. Baek, H. W. Jang, L. J. Belenky, M. Lyubchenko, and C.-B. Eom, Adv. Mater. **22**, 759 (2010).

11) Y. Noro and S. Miyahara, J. Phys. Soc. Jpn. **27**, 518 (1969).

12) T. Moriya, *Spin Fluctuations in Itinerant Electron Magnetism* (Springer, Heidelberg, 1985) Chap. 5.

13) G. Cao, S. McCall, M. Shepard, J. E. Crow, and R. P. Guertin, Phys. Rev. B **56**, 321 (1997).

14) H. Ohnishi, Y. Kondo, and K. Takayanagi, Nature **395**, 780 (1998).

15) A. I. Yanson, G. Rubio Bollinger, H. E. van den Brom, N. Agraït, and J. M. van Ruitenbeek, Nature **395**, 783 (1998).

16) D. J. Singh, J. Appl. Phys. **79**, 4818 (1996).

17) J. M. Rondinelli, N. M. Caffrey, S. Sanvito, and N. A. Spaldin, Phys. Rev. B **78**, 155107 (2008).

18) C. Etz, I. V. Maznichenko, D. Böttcher, J. Henk, A. N. Yaresko, W. Hergert, I. I. Mazin, I. Mertig, and A. Ernst, Phys. Rev. B **86**, 064441 (2012).

19) O. Grånäs, I. DiMarco, O. Eriksson, L. Nordström, and C. Etz, Phys. Rev. B **90**,

165130 (2014).

20) G. Wexler, Proc. Phys. Soc. **89**, 927 (1966).

21) Yu. G. Naidyuk and I. K. Yanson, *Point-Contact Spectroscopy* (Springer, Heidelberg, 2005) Chap. 2-3.

22) A. F. Marshall, L. Klein, J. S. Dodge, C. H. Ahn, J. W. Reiner, L. Mieville, L. Antagonazza, A. Kapitulnik, T. H. Geballe, and M. R. Beasley, J. Appl. Phys. **85**, 4131 (1999).

23) I. Asulin, O. Yuli, G. Koren, and O. Millo, Phys. Rev. B **74**, 092501 (2006).

24) M. Feigenson, J. W. Reiner, and L. Klein, Phys. Rev. Lett. **98**, 247204 (2007).

25) M. N. Baibich, J. M. Broto, A. Fert, F. Nguyen Van Dau, F. Petroff, P. Etienne, G. Creuzet, A. Friederich, and J. Chazelas, Phys. Rev. Lett. **61**, 2472 (1988).

26) A. E. Berkowitz, J. R. Mitchell, M. J. Carey, A. P. Young, S. Zhang, F. E. Spada, F. T. Parker, A. Hutten, and G. Thomas, Phys. Rev. Lett. **68**, 3745 (1992).

27) J. Q. Xiao, J. S. Jiang, and C. L. Chien, Phys. Rev. Lett. **68**, 3749 (1992).

28) K. Sekiguchi, A. Yamaguchi, H. Miyajima, A. Hirohata, and S. Usui, Phys. Rev. B **78**, 224418 (2008).
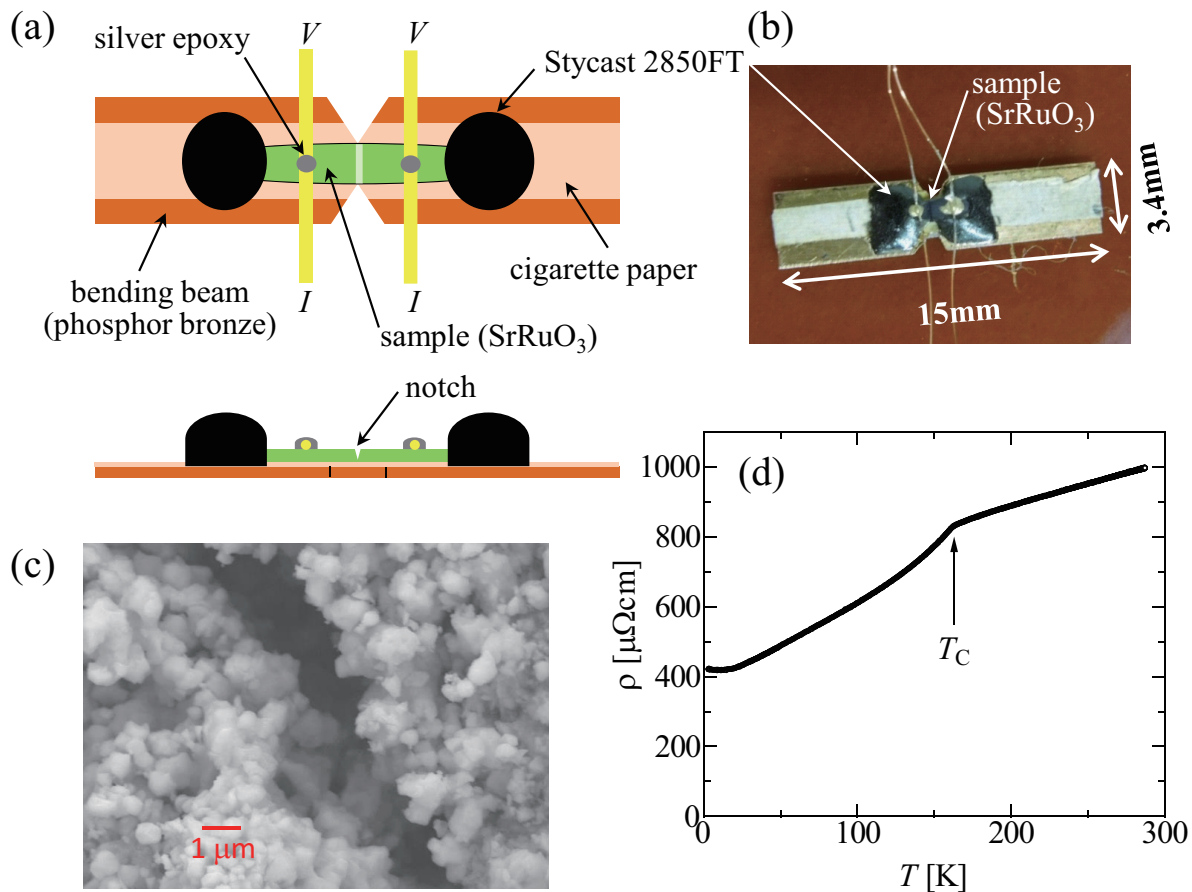
Fig. 1. (Color online) (a) Schematics of the MCBJ sample of SrRuO$_3$ [top view (upper) and side view (lower)]. (b) Photograph of the MCBJ sample on the bending beam. (c) SEM image of sample S1 after the MCBJ experiment. A breakage line can be seen at the center. (d) Bulk ρ - T data for polycrystalline SrRuO$_3$.
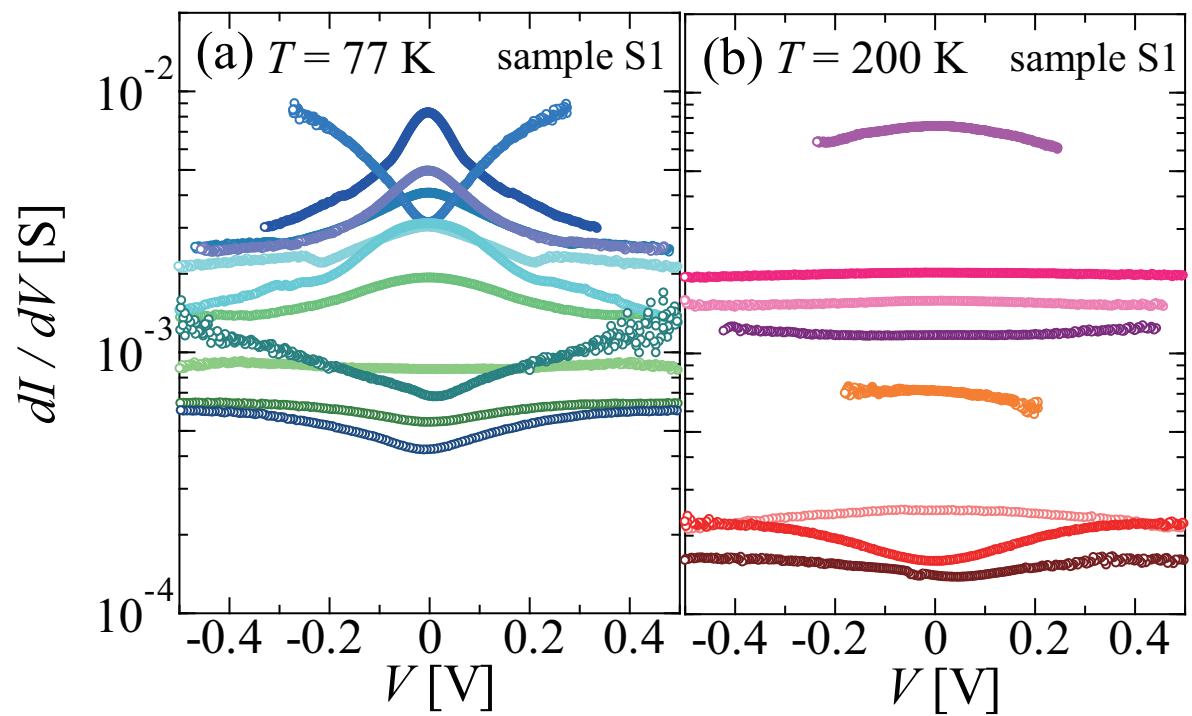
Fig. 2. (Color online) (a) dI/dV - V data of SrRuO$_3$ sample S1 obtained at 77 K (below T_C), and (b) the corresponding data obtained at 200 K (above T_C). Note the logarithmic scale on the vertical axis.
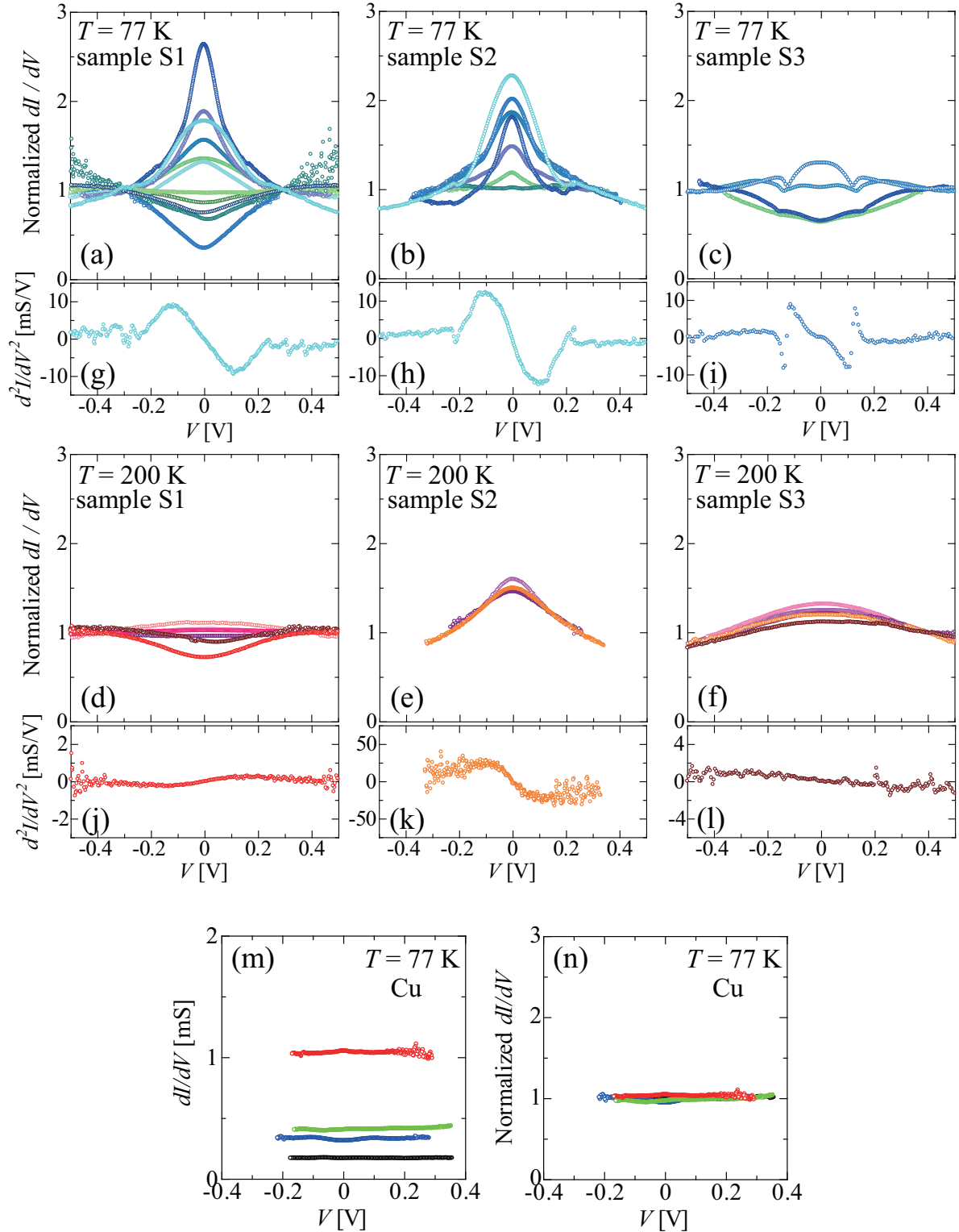
Fig. 3. (Color online) (a)-(f) Normalized dI/dV - V and (g)-(l) selected d^2I/dV^2 - V (with corresponding color) for SrRuO$_3$. The dI/dV - V data are normalized at ~ 0.3–0.4 V. The d^2I/dV^2 - V spectra are numerical derivatives of raw dI/dV data with respect to V. Data for sample S1 at (a, g) 77 K and (d, j) 200 K. Data for sample S2 at (b, h) 77 K and (e, k) 200 K. Data for sample S3 at (c, i) 77 K and (f, l) 200 K. (m) Raw dI/dV data and (n) normalized dI/dV - V for nonmagnetic Cu at 77 K.
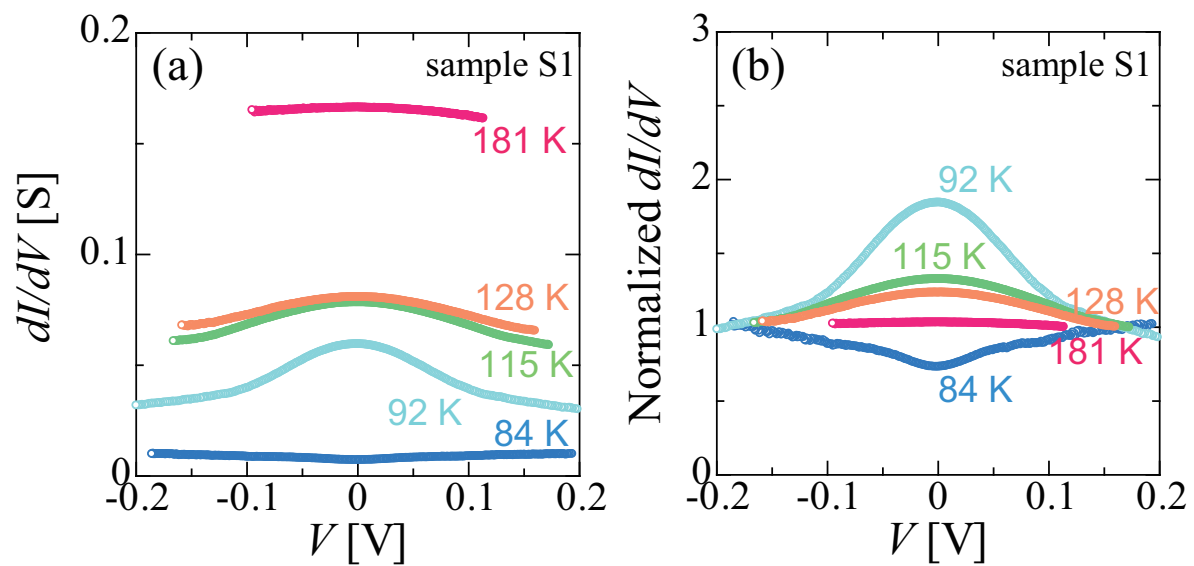
Fig. 4. (Color online) Temperature variations of dI/dV - V for SrRuO$_3$ sample S1 [(a) raw data and (b) normalized data].
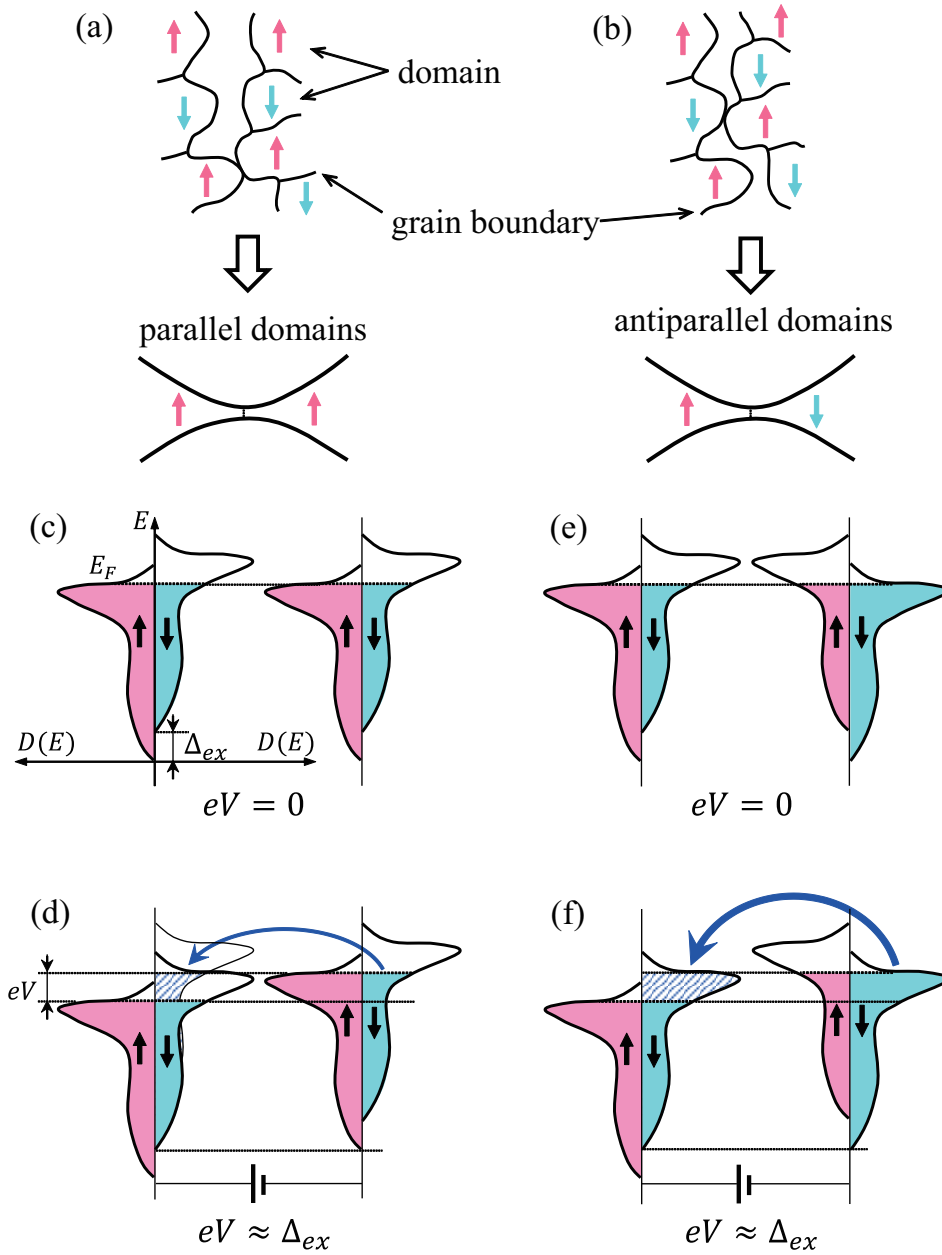
Fig. 5. (Color online) Schematics of junctions consisting of SrRuO$_3$ grains and their domain configurations in (a) parallel and (b) antiparallel case. Schematic energy bands of two electrodes on both sides of the junctions in (c, d) the parallel domain and (e, f) the antiparallel domain configurations. The dotted lines indicate the Fermi levels. The bias voltage V shifts the energy level [(c, e) $V = 0$, (d, f) $V \approx \Delta_{ex}/e$]. Δ_{ex} is the band splitting energy due to ferromagnetism. The blue hatched areas are guides to show the overlapping of the down-spins under a bias voltage of Δ_{ex}/e.